Indium-modified Yb:KLu(WO_4)$_2$ crystal: Growth, spectroscopy and laser operation

J. M. Serres[1], X. Mateos[1,2,*], P. Loiko[3], U. Griebner,[2] V. Petrov[2], K. Yumashev[4], M. Aguiló[1] and F. Díaz[1]

[1]Física i Cristal·lografia de Materials i Nanomaterials (FiCMA-FiCNA), Universitat Rovira i Virgili (URV), Campus Sescelades, c/ Marcel·lí Domingo, s/n., Tarragona E-43007, Spain
[2]Max Born Institute for Nonlinear Optics and Short Pulse Spectroscopy, 2A Max-Born-Str., Berlin D-12489, Germany
[3]ITMO University, 49 Kronverkskiy pr., St. Petersburg 197101, Russia
[4]Center for Optical Materials and Technologies (COMT), Belarusian National Technical University, 65/17 Nezavisimosti Ave., Minsk 220013, Belarus

*Corresponding author, e-mail: xavier.mateos@urv.cat, mateos@mbi-berlin.de

Abstract. We report on the growth, spectroscopic and laser characterization of a novel monoclinic laser crystal, Yb,In:KLu(WO_4)$_2$ (Yb,In:KLuW). The absorption, stimulated-emission and gain cross-section spectra of 3.5 at.% Yb, 5.5 at.% In-doped KLuW are determined at room temperature with polarized light and compared with those for Yb,In:KYW, as well as singly Yb-doped KLuW and KYW crystals. It is found that the introduction of In results in a decrease of the transition cross-sections and in a spectral broadening of the absorption and emission bands. Such a broadening is more pronounced for light polarization $E \parallel N_p$. For Yb,In:KLuW, the maximum σ_{abs} is 9.9×10^{-20} cm^2 at 980.9 nm for $E \parallel N_m$ and the corresponding bandwidth of the absorption peak is 3.7 nm. The radiative lifetime for Yb^{3+} ions is 237±5 μs. The stimulated-emission cross-sections are $\sigma_{SE}(m) = 2.4\times10^{-20}$ cm^2 at 1022.4 nm and $\sigma_{SE}(p) = 1.3\times10^{-20}$ cm^2 at 1039.1 nm corresponding to an emission bandwidth of >30 nm and >35 nm, respectively. The diode-pumped N_g-cut Yb,In:KLuW microchip laser generated 4.11 W at 1042-1048 nm with a slope efficiency of 78%. The Yb,In:KLuW crystal is very promising for the generation of sub-100 fs pulses in mode-locked lasers due to its broadband emission characteristics.

Keywords: monoclinic double tungstates, absorption, luminescence, ytterbium, diode-pumped laser

1. Introduction

Ytterbium-doped monoclinic double tungstates (DTs) with the chemical formula Yb:$KRE(WO_4)_2$ or shortly Yb:KREW where RE stands for a "passive" trivalent ion like Gd, Y or Lu, are attractive materials for efficient lasers emitting at ~1 μm [1,2] and operating in the continuous-wave (CW) [3,4], Q-switched [5,6] and mode-locked regimes [7,8]. This is related to the intrinsic spectroscopic features of the Yb^{3+} ions and physical characteristics of DTs. In this sense, the Yb^{3+} ion shows a simple energy-level scheme without parasitic processes like up-conversion, it provides low quantum defect due to the direct excitation to the upper laser level and, hence, reduced heat loading. Such features lead to high laser efficiencies approaching the Stokes limit and the possibility of power scaling due to the weak thermal effects. When introduced in the low-symmetry KREW host, Yb^{3+} ions show high transition cross-sections (absorption and emission) for polarized light, as well as relatively broad spectral bands [9,10]. Due to the large RE^{3+}-RE^{3+} ion separation, high Yb^{3+} doping levels are possible still with a weak concentration-quenching [11]. Although the thermal conductivity of monoclinic DTs is moderate (~3 W/mK) [12], there exists a special "athermal" crystal orientation [13] that produces a relatively weak thermal lens [14].

The above mentioned properties of Yb-doped DTs and, in particular, the large emission bandwidths for the Yb^{3+} ion have defined their potential for passively mode-locked lasers emitting sub-100 fs pulses at 1.02-1.04 μm. Mode-locking of Yb:KGdW [15], Yb:KYW [16] and Yb:KLuW [7] crystal lasers has previously been realized. When using a semiconductor saturable absorber mirror (SESAM), such lasers generated pulses as short as 100 fs, 101 fs and 81 fs, respectively. A Kerr-lens mode-locked Yb:KYW laser provided 71 fs pulses [17]. The possibility of power scaling of mode-locked thin-disk Yb:DT oscillators was also demonstrated [18].

DTs with Gd, Y or Lu "passive" host ions are isostructural and can form isostructural solid state solutions with composition $KGd_aY_bLu_cW$. To date, this approach was mainly used to optimize the lattice mismatch and refractive index contrast in μm-thickness DT waveguides [19,20]. However, such "mixed" materials can be of interest for mode-locking due to the broadening of the emission bands caused by distortion of the local site symmetry for the active ions as demonstrated in other hosts [21,22].

Recently, it was proposed to introduce trivalent Indium (In^{3+}) as an additional "passive" ion into the DT lattice (in the particular case of KYW) resulting in a monoclinic $KY_aIn_bYb_cW$ structure [23], which can provoke the desired broadening of the emission bandwidth for the Yb^{3+} ion due to the relatively small ionic radius of the VIII-fold O^{2-}-coordinated In^{3+} (0.92 Å) as compared to that of Y^{3+} (1.019 Å) and Yb^{3+} (0.985 Å). The growth, low-temperature spectroscopy, CW and mode-locked operation of In-modified Yb:KYW was reported in [23,24]. In the mode-locking regime, 96 fs pulses were generated with an average output power of 131 mW and a repetition rate of 103.5 MHz. In the CW regime, the Yb,In:KYW laser generated ~0.5 W of output power with a maximum slope efficiency of 69%. Although sub-100 fs pulses were obtained from the Yb,In:KYW mode-locked laser, the spectroscopic background supporting the potential for pulse shortening was not presented completely and, in particular, at room-temperature where laser operation was achieved.

In the preset work, we present a detailed spectroscopic study of a novel DT laser crystal, Yb,In:KLuW in comparison with Yb,In:KYW and singly Yb-doped KLuW and KYW crystals. Highly efficient multi-watt CW laser operation of the Yb,In:KLuW crystal is also demonstrated.

2. Crystal growth

The studied crystals were grown by the Top-Seeded Solution Growth Slow Cooling (TSSG - SC) method using potassium ditungstate, $K_2W_2O_7$, as a solvent. The growth was performed without pulling. Details about the growth procedure can be found elsewhere [1]. The solution mixture (12 mol% KREW as a solute - 88 mol% $K_2W_2O_7$ as a solvent, 200 g in weight), placed in a platinum crucible of 50 cm diameter and 50 cm height, was inserted into a vertical tubular furnace. The precursor materials, K_2CO_3, WO_3, and Ln_2O_3 (Ln = Lu, Y, In, Yb), were from Aldrich, Fluka and Metall rare earth Ltd., with analytical grade of purity. The concentration of Yb in the solution was 2.5 at.% and the concentration of In was 10 at.%. The solution was homogenized at 50 K above the saturation temperature for 7-8 h. A KLuW or KYW seed oriented along the [010] crystallographic axis was attached to a Pt holder, perpendicular to the solution surface. The temperature gradient in the solution was ~ 1 K/cm in the vertical and radial directions. The solution temperature was decreased by ~20 K at a rate of 0.1 K/h. The growth rate was ~19 mg/h. The seed was rotated at 40 rpm in order to enhance the mass and heat transfer in the solution and to avoid inclusions during the crystal growth. After 8–10 days of growth, the crystals were slowly removed from the solution at a rate of 1 mm per 10 min until losing contact with the solution, then the furnace was cooled down to room temperature at 25 K/h to avoid thermal shocks.

The as-grown crystal bulks were colorless and contained no inclusions, Fig. 1(a,b). Their structure was confirmed with X-ray powder diffraction (monoclinic, space group C^6_{2h} – *C2/c*). The morphology of the grown crystals was similar to the one observed previously for undoped KLuW [1], with the developed faces being {110}, $\{\bar{1}11\}$, {010} and {310}, Fig. 1(c). The weight of the grown crystals was about 2-7 g and the typical dimensions were about 7-9 mm along the ***a****-axis, 5-7 mm along the ***b***-axis and 15-30 mm along the ***c***-axis. The inner part of the boule (close to the seed) contained few cracks most probably related to the lattice mismatch between the seed (undoped KLuW or KYW) and the growing crystal, and facilitated by non-uniform inclusion of In. The outer part of the crystal was of good optical quality and contained no cracks. From the outer part of the boule, we cut 3×2.5×3 mm^3 oriented samples (see below), whose composition was studied with Energy-Dispersive X-ray (EDX) spectroscopy using Electron Scanning Environmental Microscope (ESEM) equipped with an Inca microanalyzer (Oxford Instruments). The results are shown in Table 1. The actual doping level with Yb^{3+} was 3.5 at.% (for Yb,In:KLuW) and 3.2 at.% (for Yb,In:KYW) which corresponds to segregation coefficients K_{Yb} = 1.40 and 1.28, respectively. Consequently, the concentration of Yb^{3+} ions was 2.27 and 1.98×10^{20} cm^{-3}, respectively (according to the crystal density, ρ = 7.62 and 6.50 g/cm^3). The actual doping level with In^{3+} was 5.5 at.% (for Yb,In:KLuW) and 5.2 at.% (for Yb,In:KYW). The distribution of Yb^{3+} and In^{3+} ions in the studied samples was uniform and the spatial variation of the doping level did not exceed 0.4 at.%. The stoichiometric formulas for the grown crystals are $KLu_{0.91}In_{0.055}Yb_{0.035}(WO_4)_2$ and $KY_{0.916}In_{0.052}Yb_{0.032}(WO_4)_2$.

Monoclinic DTs are optically biaxial [1]. Their optical properties are described in the frame of the optical indicatrix with the three mutually orthogonal principal axes, N_p, N_m and N_g (the corresponding refractive indices are $n_p < n_m < n_g$). The N_p-axis is parallel to the *b*-axis and the two remaining principal axes are located in the *a-c* plane, Fig. 1(d). In particular, the angle $N_g \wedge c$ = 18.5° for KYW and KLuW crystals at ~1 μm. From the as-grown bulk, samples were cut for spectroscopic

studies. They were oriented in the frame of the optical indicatrix with dimensions of 3(N_p)×2.5(N_m)× 3(N_g) mm^3 and all side polished in order to access the principal light polarizations, $E \parallel N_p$, N_m and N_g.

3. Experimental

3.1 Spectroscopy

The absorption spectra were measured with polarized light using a Varian CARY-5000 spectrophotometer with a spectral resolution of 0.02 nm and a Glan-Taylor prism. The absorption cross-section was calculated from the measured absorption coefficient as $\sigma_{abs} = \alpha/N_{Yb}$. For comparison, we recorded the same data for singly doped 3 at.% Yb:KLuW and 3 at.% Yb:KYW crystals.

The luminescence of Yb^{3+} ions was excited at ~955 nm by a CW InGaAs laser diode. The emission spectra were measured with a grating monochromator (resolution, 0.1 nm), a Hamamatsu G5851 TE-cooled InGaAs PIN photodiode and a lock-in amplifier.

To determine the radiative lifetime of Yb^{3+} ions τ_{rad} in the studied crystals, we employed the powder method which allows one to avoid the impact of radiation self-trapping. The crystal sample was finely powdered and immersed in glycerin. The luminescence was excited at 980 nm by a ns optical parametric oscillator Lotis TII LT-2214 and detected at 1040 nm with a grating monochromator (resolution, ~1 nm), the same Hamamatsu photodetector and a 500 MHz digital oscilloscope. The decay curve was approximated according to a single-exponential law, $I_{lum}(t) = I_0\exp(-t/\tau)$. The content of the powder was reduced until no effect on the measured decay time could be seen. This occurred for ~10 wt.% of powder in the solution. The corresponding decay time was considered as τ_{rad}.

Raman spectra were measured with polarized light using a Renishaw inVia Raman microscope with a x50 objective. The excitation wavelength and the spectral resolution were 632.8 nm (He–Ne laser) and 0.1 cm^{-1}, respectively.

3.2 Laser set-up

Laser operation of the Yb,In:KLuW crystal was studied in a microchip set-up. The 1.5 mm thick crystal was cut along the N_g-axis of the optical indicatrix because this cut provides a positive sign of the thermal lens which is required for stabilization of the microchip cavity [25]. Both 3.0(N_m)×3.0(N_p) mm^2 input and output faces of the crystal were polished to laser quality and remained uncoated. The crystal was wrapped with Indium foil and mounted in a Cu-holder water-cooled down to 12 °C. The laser cavity consisted of a flat pump mirror (PM) which was antireflection (AR) coated for 0.78–0.99 µm and high-reflection (HR) coated for 1.01–1.23 µm, and a flat output coupler (OC) which provided a transmission of T_{OC} = 0.5%, 1%, 5% or 10% at 1.0–1.23 µm. Both PM and OC were attached to the surfaces of the laser crystal without air gaps resulting in a total geometrical cavity length of 1.5 mm. The crystal was pumped by a fiber-coupled InGaAs laser diode (core diameter: 200 µm, N.A.: 0.22) emitting unpolarized radiation at ~978 nm (M^2 = 71). The pump radiation was focused into the crystal with a lens assembly (imaging ratio: 1:1, focal length: 30 mm) providing a pump spot radius in the crystal of w_p = 100 µm with a Rayleigh length of 1.7 mm. Due to the partial reflection of the OC at the pump wavelength (R ~90%), the crystal was pumped in a double-pass. The total absorption in the crystal under lasing conditions was 51%.

The spectra of the laser emission were detected with a spectrometer (APE GmbH, model Wavescan RS232) having a spectral resolution of 0.05 nm. The output beam profile was measured with

a FLIR SC7210 thermal imaging camera (pixel size: 30 μm) at a distance of 15 cm from the OC. To measure the M^2 parameter of the laser beam, it was focused with a 60 mm lens and for the determination of the beam caustic corresponding to the N_m and N_p-axes the moving knife method was applied.

4. Results and discussion

4.1 Absorption

The absorption cross-sections of Yb,In:KLuW and Yb,In:KYW for light polarizations $E \parallel N_m$ and $E \parallel N_p$ which are interesting for laser applications are shown in Fig. 2(a,b) and Fig. 3(a,b), respectively. In Table 2, we compare the absorption characteristics of these crystals with those determined for singly Yb-doped KLuW and KYW. All crystals possess strong anisotropy of the absorption which is much higher for $E \parallel N_m$ than for $E \parallel N_p$, a characteristic feature of Yb-doped DTs [1,9]. In particular, the ratios of the peak absorption cross-sections at the zero-phonon line are $\sigma_{abs}(m):\sigma_{abs}(p)$ = 7:1 at 980.8 nm for Yb,In:KLuW and 8:1 at 981.0 nm for Yb,In:KYW. The absolute values of σ_{abs} are somewhat lower for Yb,In:KLuW ($\sigma_{abs}(m) = 9.9\times10^{-20}$ cm^2) compared to Yb,In:KYW ($\sigma_{abs}(m) = 10.9\times10^{-20}$ cm^2). This follows the tendency for singly Yb-doped crystals (as observed in the present study). In addition, all values of σ_{abs} for In-modified crystals are ~20% lower than those for singly Yb-doped crystals.

Concerning the linewidth of the absorption peak, the full width at half maximum, FWHM, is ~1.5 times broader for $E \parallel N_p$ than for $E \parallel N_m$ (for all studied crystals). For Yb,In:KLuW, the introduction of Indium results in a slight (~0.2 nm) blue-shift of the position of the zero-phonon line. In addition, Indium broadens the linewidth, which is less pronounced for $E \parallel N_m$ (FWHM = 3.7 nm compared to 3.5 nm for singly doped Yb:KLuW) than for $E \parallel N_p$ (FWHM = 6.3 nm, i.e. ~1.5 times broader than in Yb:KLuW for which it is 4.1 nm). For Yb,In:KYW, a similar ~0.2 nm blue-shift of the absorption peak is detected whilst the introduction of Indium leads to a slight decrease of the bandwidth for both light polarizations. Finally, the FWHM for Yb,In:KYW amounts to 4.1 nm (N_m) and 5.5 nm (N_p).

4.2 Luminescence

The stimulated-emission (SE) cross-sections σ_{SE} for the studied crystals were calculated with the modified reciprocity method [26]:

$$\sigma^i_{SE}(\lambda) = \frac{1}{8\pi n_i^2 \tau_{rad} c} \frac{3\sigma^i_{abs}(\lambda)\exp(-hc/(kT\lambda))}{\sum_{i=p,m,g} \int \lambda^{-4} \sigma^i_{abs}(\lambda)\exp(-hc/(kT\lambda))\mathrm{d}\lambda}. \quad (1)$$

Here, σ^i_{SE} and σ^i_{abs} (i = p, m or g) are the SE and absorption cross-sections for the i-th principal light polarization, h is the Planck constant, c is the speed of light, k is the Boltzmann constant, λ is the wavelength, n_i is the refractive index of the crystal for the i-th polarization, τ_{rad} is the radiative lifetime of the emitting state ($^2F_{5/2}$ state of Yb^{3+}). The values of n_i for DTs codoped with Yb-In and doped only with Yb are very close [24].

The measured decay curves for the powdered Yb,In:KLuW and Yb,In:KYW crystals are shown in Fig. 4. They are clearly singly exponential, the accuracy of the fit is $R^2 > 0.99$. The radiative lifetime is 237±5 μs and 231±5 μs, respectively.

The SE cross-sections of Yb,In:KLuW and Yb,In:KYW crystals for light polarizations $E \parallel N_m$ and $E \parallel N_p$ are shown in Fig. 2(a,b) and Fig. 3(a,b), respectively. In Table 3, we also compare the emission characteristics of In-modified Yb:KLuW and Yb:KYW with those determined for the singly Yb-doped crystals. The maximum σ_{SE} in the Yb-doped DTs typically corresponds to the zero-phonon line, but it is typically not accessible in a real bulk laser due to a strong reabsorption loss. Thus, we considered a red-shifted local peak in the SE cross-sections spectra where laser oscillation typically occurs. All crystals show anisotropy of the SE cross-sections which are much higher for $E \parallel N_m$ than for $E \parallel N_p$. In particular, the ratios of the local-peak cross-sections are $\sigma_{SE}(m):\sigma_{SE}(p)$ = 1.8:1 for Yb,In:KLuW and 1.9:1 for Yb,In:KYW. The absolute values of σ_{SE} are lower for Yb,In:KLuW, for which $\sigma_{SE}(m) = 2.4\times10^{-20}$ cm^2 at 1022.4 nm compared to Yb,In:KYW for which $\sigma_{SE}(m) = 3.0\times10^{-20}$ cm^2 at 1025.2 nm. All values of σ_{SE} for In-modified crystals are ~20% lower than those for singly Yb-doped crystals. The reabsorption in In-modified crystals, expressed by the absorption cross-section at the emission wavelength (cf. Table 3) is 0.2 ...0.3×10^{-20} cm^2 for $E \parallel N_m$ and ~0.1×10^{-20} cm^2 for $E \parallel N_p$.

For the three-level Yb^{3+} ion, due to the overlap of the absorption and emission bands, an important parameter is the gain cross-section, σ_g:

$$\sigma_g^i(\lambda) = \beta\sigma_{SE}^i(\lambda) - (1-\beta)\sigma_{abs}^i(\lambda), \quad (2)$$

where β is the inversion ratio, $\beta = N_2/N_0$ with N_2 and N_0 denoting the number of ions in the upper laser level ($^2F_{5/2}$) and the total number of ions, respectively.

The gain spectra of Yb,In:KLuW and Yb,In:KYW for light polarizations $E \parallel N_m$ and $E \parallel N_p$ are shown in Fig. 2(c,d) and Fig. 3(c,d), respectively. In the following, we describe the spectral behavior of the gain in Yb,In:KLuW. For $E \parallel N_m$ and low inversion ($\beta < 0.1$), a broad and structureless gain spectrum spanning from 1040 to 1080 nm is observed. For $\beta > 0.1$, the spectrum exhibits two local peaks at ~1023 and 1029 nm, and for $\beta > 0.4$, laser emission is most likely to occur at ~999 nm, corresponding to the formation of a local peak at even shorter wavelengths. At low inversion, the shape of the gain spectrum for $E \parallel N_p$ is very similar to the one for $E \parallel N_m$ and $\sigma_g(p) \geq \sigma_g(m)$ is fulfilled. For $\beta > 0.1$, the $E \parallel N_p$ spectrum contains a local peak at ~1039 nm which dominates also for high inversion levels. From the gain spectra, we also estimated the bandwidth of the gain peak, $\Delta\lambda_g$ (FWHM), see Table 3.

In addition, we directly measured the emission spectra for the studied crystals. The results are shown in Fig. 5 both for Yb,In-codoped and singly Yb-doped crystals for light polarizations $E \parallel N_m$ and $E \parallel N_p$. The determined bandwidths of the emission bands, $\Delta\lambda_{lum}$, are also compiled in Table 3.

By analyzing both $\Delta\lambda_g$ and $\Delta\lambda_{lum}$, one can see the role of Indium on the broadening of the emission bands in Yb:KLuW and Yb:KYW. From Table 3, we indeed can conclude that the introduction of Indium leads to a broadening of the emission bands. This effect is more pronounced for $E \parallel N_p$ (the broadening is 7-8 nm with respect to singly Yb-doped crystal) than for $E \parallel N_m$ (where the broadening is 3-4 nm). The impact of In is more pronounced for Yb,In:KYW which is attributed to the larger difference of ionic radii of Y^{3+} (1.019 Å) and In^{3+} (0.92 Å) as compared with Lu^{3+} (0.977 Å) and In^{3+} (0.92 Å). For Yb,In:KLuW, $\Delta\lambda_{lum}$ amounts to 31.2 nm for $E \parallel N_m$ and 36.3 nm for $E \parallel N_p$. The determined spectral features indicate that Yb,In:KLuW is interesting for applications in femtosecond mode-locked lasers capable of generating shorter pulses than that based on Yb:KLuW.

4.3 Raman spectroscopy

The monoclinic DTs and in particular, KLuW, are well-known Raman-active materials [27,28]. The polarized Raman spectra of Yb,In:KLuW for *x*(*yy*)*x* geometries (where *x* and *y* = *p, m* or *g*) are shown in Fig. 6. All spectra are normalized to unity. The phonons below 270 cm^{-1} are assigned to external lattice modes associated with the translational motion of the cations of the structure (K^+, Lu^{3+}, In^{3+}, Yb^{3+} and W^{6+}) and the rotational motion of the WO_6 groups in the unit cell. The bending modes are observed in the 270–460 cm^{-1} range, and the stretching modes in the 400–1000 cm^{-1} range. The bands in the 430–750 cm^{-1} region, which are not observed for scheelite-like structures (e.g., $CaWO_4$) with isolated WO_4 tetrahedra, are related to double oxygen bridge vibrations [29]. The spectra of Yb,In:KLuW are strongly polarized. The most intense stretching modes that are suitable for Raman self-conversion appear at 906.5 cm^{-1} (assigned as ν(W–O)/ν_1) and 755.1 cm^{-1} (ν(WOOW)*ν(W–O)/ν_3^0). Here, W–O stands for tungsten-oxygen bonds, WOOW is the double oxygen bridge and * indicates the coupling of the vibrations. The linewidths (FWHM) of these lines are 10.9 and 16.1 cm^{-1}, respectively. For the high laser gain light polarization $E \parallel N_m$, the ~907 cm^{-1} mode dominates both for N_p-cut and N_g-cut crystals.

In Fig. 7, we compared the Raman spectra of Yb,In:KLuW, Yb,In:KYW and Yb:KLuW crystals (for the *g*(*mm*)*g* geometry). The spectra of all three crystals are similar confirming their purely monoclinic structure. In Table 4, we also analyzed the two most intense Raman lines for these crystals. For Yb:KLuW, the introduction of Indium results in a red-shift of the Raman lines (from 908.1 to 906.5 cm^{-1} and from 758.2 to 755.1 cm^{-1}) together with their broadening (the increase of the linewidth is ~1 cm^{-1}). As compared with Yb,In:KYW, the Raman bands for Yb,In:KLuW are broader which should result in shorter dephasing times.

4.4 Laser operation

The input-output dependences for the Yb,In:KLuW microchip laser are shown in Fig. 8(a). Maximum output power of 4.11 W was extracted with T_{OC} = 5% at 1042-1048 nm (multi-peak spectrum, see Fig. 8(b)) corresponding to a slope efficiency η = 78% (with respect to the absorbed pump power). The laser threshold was at P_{abs} = 1.5 W and the optical-to-optical efficiency η_{opt} amounted to 56%. For T_{OC} = 10%, the slope efficiency was slightly smaller (η = 77%) and the laser oscillated at shorter wavelengths, 1031-1036 nm. However, due to a higher threshold (1.8 W) the output power reached only 3.85 W. In both cases, the laser emission was linearly polarized parallel to the N_m-axis of the optical indicatrix. This is in agreement with the gain curves for Yb,In:KLuW, see Fig. 2(c,d). As high T_{OC} corresponds to high inversion, particularly, the oscillation state $E \parallel N_m$ will be selected due to the anisotropy of the gain. With the increase of output coupling the emission wavelength will be blue-shifted.

The maximum pump level for the microchip laser was limited to avoid thermal fracture of the crystal. The output performance of the Yb,In:KLuW laser was very similar to the one achieved with singly Yb-doped 1.5 mm-long 3 at.% Yb:KLuW crystal studied for comparison. For both crystals, high risk of thermal fracture was observed at a very similar pump level ($P_{abs} \geq 10$ W).

The slope efficiency of an Yb laser can be theoretically expressed as [30]:

$$\eta = \eta_{mode}\eta_{St}\eta_q\eta_{out}, \quad (3)$$

where η_{mode} is the mode-matching efficiency, $\eta_{St} = \lambda_p/\lambda_L$ is the Stokes efficiency (λ_p and λ_L are the pump and laser wavelength, respectively), η_q is the quantum efficiency of excitation of Yb^{3+} ions (the number

of emitted photons due to one pump photon) and η_{out} is the cavity output-coupling efficiency (relation of useful losses to the total cavity losses, $\eta_{out} = \ln[1-T_{OC}]/\ln[(1-T_{OC})*(1-L)]$ where L is the roundtrip passive loss).

For Yb^{3+} ion in DTs, the energy gap between the $^2F_{5/2}$ excited-state and the $^2F_{7/2}$ ground-state is ~9600 cm^{-1} and it is ~10 times larger than the maximum phonon frequency of the host, ~907 cm^{-1} [1]. Thus, one can expect η_q approaching 1. The considered laser provided a good mode-matching with an overlap integral for the pump and laser modes of ≈0.86 (as calculated from the parameters of the thermal lens in Yb:KLuW [14]). The passive losses in the crystal were estimated to be as low as $L \approx 1\times10^{-3}$, so that $\eta_{out} = 0.98$ (for $T_{OC} = 5\%$). The Stokes efficiency amounted to $\eta_{St} = 0.93$ ($\lambda_p = 978$ nm and $<\lambda_L> = 1050$ nm). Therefore, the theoretical value of the slope efficiency amounted to 79±1% (for $T_{OC} = 5\%$) which is in good agreement with the experimental data.

For low T_{OC}, more complicated polarization behavior was observed. For T_{OC} =1%, two polarization states, $E \parallel N_m$ and $E \parallel N_p$, were coexisting. The maximum output power was 1.95 W with η = 46% and the laser threshold was at $P_{abs} = 1.3$ W. The output dependence was linear up to P_{abs} ~5.5 W where thermal roll-over was observed. However, the respective fractions of output power corresponding to N_m and N_p-polarized oscillation states, as well as the emission spectrum changed with the pump level, see Fig. 9. Close to the threshold, the laser output was predominantly polarized along the N_m-axis and the laser emitted at 1048-1053 nm. At high pump levels almost purely N_p-polarized emission was detected corresponding to longer emission wavelengths, 1053-1062 nm. At intermediate pump levels, the coexistence of both oscillation states resulted in a broad emission spectrum. For $T_{OC} = 0.5\%$, the laser emission was again linearly polarized but corresponding to $E \parallel N_p$. The laser generated a maximum output power of 1.14 W at 1052-1071 nm with η = 38% and the threshold was as low as 1.1 W.

The coexistence of orthogonal polarization states results in broadening of the emission spectrum or dual-wavelength operation which is an effect often observed in Yb^{3+}-doped anisotropic materials [25,31]. It is explained by the anisotropy of the gain and the parameters of thermal lensing [32]. For low T_{OC} (and, hence, low inversion), the gain in Yb,In:KLuW is close or even higher at some particular wavelengths for light polarization $E \parallel N_p$ as compared with $E \parallel N_m$. In addition, the optical power of the thermal lens for an N_g-cut crystal is positive for both N_m and N_p-oscillation states. This means that both of them can stabilize the plano-plano microchip cavity. Moreover, the thermal lens for light polarization $E \parallel N_p$ is weaker and introduces lower diffraction loss. Thus, for low T_{OC}, the generation of N_p-polarized output is more favorable which is indeed observed experimentally for $T_{OC} = 0.5\%$. For $T_{OC} = 1\%$, the polarization switching is induced by the stronger thermal lens whose optical power is pump-dependent.

The Yb,In:KLuW laser generated a nearly-circular laser beam corresponding to TEM_{00} mode, Fig. 10(a). The M^2 factors for the N_m and N_p directions were determined to be as low as 1.15 and 1.07, respectively (for $T_{OC} = 5\%$, at $P_{abs} = 7$ W), see Fig. 10(b). Good quality of the laser beam is consistent with the low astigmatism of the thermal lens as determined for N_g-cut Yb:KLuW [25] and shows that In modification does not result in additional defects and growth stresses in the crystal which can lead to beam distortion.

For comparison, we studied also the microchip laser performance of Yb,In:KYW. For $T_{OC} = 5\%$, it generated 1.07 W at 1033-1037 nm with a slope efficiency of only 54% (the laser output was linearly polarized, $E \parallel N_m$). The laser threshold was at $P_{abs} = 2.2$ W and $\eta_{opt} = 23\%$. Further power scaling was limited by stress fracture of the crystal the probability for which was found to be very high for $P_{abs} \geq 5$

W. The M^2 factor for the laser beam reached 1.25. We attribute this degradation of the laser performance and reduced stress fracture limit (as compared to Yb,In:KLuW) to higher internal losses in Yb,In:KYW.

5. Conclusion

We have successfully grown a new laser crystal, 3.5 at.% Yb, 5.5 at.% In:$KLu(WO_4)_2$ (Yb,In: KLuW) which belongs to the family of the monoclinic double tungstates. The introduction of Indium allows one to keep the advantage of high transition cross-sections in polarized light together with the broadening of the emission bands which is of interest for application in sub-100 fs mode-locked lasers. Although the In-modification of Yb:KLuW crystal has less significant effect on the emission bandwidth as compared with Yb,In:KYW, the former material is beneficial in terms of better crystal quality and higher thermal fracture limit. The polarizations of interest for Yb,In:KLuW lasers are $E \parallel N_m$ and $E \parallel N_p$. The first one corresponds to higher absorption and stimulated-emission cross-sections, namely $\sigma_{abs} = 9.9\times10^{-20}$ cm^2 at 980.8 nm and $\sigma_{SE} = 2.4\times10^{-20}$ cm^2 at 1022.4 nm. For $E \parallel N_p$, the effect of In modification on the emission bandwidth is more pronounced (FWHM of the emission band is >35 nm). With a N_g-cut Yb,In:KLuW crystal, we have realized an efficient (slope efficiency η = 78%) diode-pumped CW microchip laser generating 4.11 W at 1042-1048 nm in a circular TEM_{00} mode with M^2 <1.15.

Further work on Yb,In:KLuW should be focused on mode-locked operation at ~1 μm for the laser polarization $E \parallel N_m$. The development of the crystal composition can be also done by the introduction of higher concentrations of In (up to 10...20 at.% still keeping the monoclinic structure). The latter was limited in the present work by the low segregation coefficient for In (K_{In} ~0.5). A higher In content may lead to a further broadening of the emission bands. However, it should be noted that the stoichiometric compound, KInW, is not isostructural to monoclinic DTs. KInW belongs to the orthorhombic class (space group D^{16}_{2h}) [33,34] and thus the increase of In doping concentration for monoclinic Yb,In:KLuW crystals is limited similarly to Yb,In:KYW [23]. Introduction of different passive ions with even larger difference of ionic radii with respect to Y^{3+} or Lu^{3+}, e.g. Sc^{3+} (ionic radius: 0.87 Å), can lead to a similar effect on the spectral bands. The growth of RE,In:KLuW crystals where RE = Tm and Ho seems to be also promising for broadband mode-locked oscillators at ~2 μm.

Acknowledgements

This work was supported by the Spanish Government under projects MAT2013-47395-C4-4-R and TEC2014-55948-R, and by the Generalitat de Catalunya under project 2014SGR1358. F.D. acknowledges additional support through the ICREA academia award 2010ICREA-02 for excellence in research. This work is part of a project that has received funding from the European Union's Horizon 2020 research and innovation programme under the Marie Skłodowska-Curie grant agreement No 657630. P.L. acknowledges financial support from the Government of the Russian Federation (Grant 074-U01) through ITMO Post-Doctoral Fellowship scheme.

References

1. V. Petrov, M. C. Pujol, X. Mateos, Ò. Silvestre, S. Rivier, M. Aguiló, R. M. Solé, J. Liu, U. Griebner, F. Díaz, Laser & Photon. Rev. 1 (2007) 179–212.
2. M. Pollnau, Y. E. Romanyuk, F. Gardillou, C. N. Borca, U. Griebner, S. Rivier, V. Petrov, IEEE J. Sel. Top. Quantum Electron. 13 (2007) 661–671.
3. J. Liu, V. Petrov, X. Mateos, H. Zhang, J. Wang, Opt. Lett. 32 (2007) 2016–2018.
4. P. A. Loiko, V. E. Kisel, N. V. Kondratuk, K. V. Yumashev, N. V. Kuleshov, A. A. Pavlyuk, Opt. Mater. 35 (2013) 582–585.
5. V. E. Kisel, A. S. Rudenkov, N. V. Kuleshov, A. A. Pavlyuk, Opt. Lett. 39 (2014) 3038–3041.
6. P. Loiko, J. M. Serres, X. Mateos, K. Yumashev, A. Yasukevich, V. Petrov, U. Griebner, M. Aguiló, F. Díaz, Opt. Lett. 41 (2016) 2620–2623.
7. U. Griebner, S. Rivier, V. Petrov, M. Zorn, G. Erbert, M. Weyers, X. Mateos, M. Aguiló, J. Massons, F. Díaz, Opt. Express 13 (2005) 3465–3470.
8. S. Pekarek, C. Fiebig, M. C. Stumpf, A. E. H. Oehler, K. Paschke, G. Erbert, T. Südmeyer, U. Keller, Opt. Express 18 (2010) 16320–16326.
9. X. Mateos, R. Solé, J. Gavaldà, M. Aguiló, J. Massons, F. Díaz, V. Petrov, U. Griebner, Opt. Mater. 28 (2006) 519–523.
10. N. V. Kuleshov, A. A. Lagatsky, V. G. Shcherbitsky, V. P. Mikhailov, E. Heumann, T. Jensen, A. Diening, G. Huber, Appl. Phys. B 64 (1997) 409-413.
11. M. C. Pujol, M. A. Bursukova, F. Güell, X. Mateos, R. Solé, J. Gavaldà, M. Aguiló, J. Massons, F. Díaz, P. Klopp, U. Griebner, V. Petrov, Phys. Rev. B 65 (2002) 165121-1-11.
12. O. Silvestre, J. Grau, M. C. Pujol, J. Massons, M. Aguilo, F. Diaz, M. T. Borowiec, A. Szewczyk, M. U. Gutowska, M. Massot, A. Salazar, V. Petrov, Opt. Express 16 (2008) 5022–5034.
13. S. Biswal, S. P. O'Connor, S. R. Bowman, Appl. Opt. 44 (2005) 3093–3097.
14. P. A. Loiko, J. M. Serres, X. Mateos, K. V. Yumashev, N. V. Kuleshov, V. Petrov, U. Griebner, M. Aguiló, F. Díaz, Laser Phys. Lett. 11 (2014) 125802-1-6.
15. G. Paunescu, J. Hein, R. Sauerbrey, Appl. Phys. B 79 (2004) 555-558.
16. P. Klopp, V. Petrov, U. Griebner, G. Erbert, Opt. Express 10 (2002) 108-113.
17. H. Liu, J. Nees, G. Mourou, Opt. Lett. 26 (2001) 1723-1725.
18. F. Brunner, T. Südmeyer, E. Innerhofer, F. Mourier-Genoud, R. Paschotta, V. E. Kisel, V. G. Shcherbitsky, N. V. Kuleshov, J. Gao, K. Contag, A. Giesen, U. Keller, Opt. Lett. 27 (2002) 1162-1164.
19. Ò. Silvestre, A. Aznar, R. Solé, M. C. Pujol, F Díaz, M Aguiló, J. Phys.: Cond. Matter 20 (2008) 225004-1-10.
20. D. Geskus, S. Aravazhi, C. Grivas, K. Wörhoff, M. Pollnau, Opt. Express 18 (2010) 8853-8858.
21. V.E. Kisel, N.A. Tolstik, A.E. Troshin, N.V. Kuleshov, V.N. Matrosov, T.A. Matrosova, M.I. Kupchenko, F. Brunner, R. Paschotta, F. Morier-Genoud, U. Keller, Appl. Phys. B 85 (2006) 581-584.

22. C. R. E. Baer, C. Kränkel, O. H. Heckl, M. Golling, T. Südmeyer, R. Peters, K. Petermann, G. Huber, U. Keller, Opt. Express 17 (2009) 10725-10730.
23. E. Castellano-Hernández, X. Han, C. Cascales, C. Zaldo, *Advanced Solid-State Lasers Congress*, G. Huber and P. Moulton, eds., OSA Technical Digest (online) (Optical Society of America, 2013), paper AW1A.2.
24. E. Castellano-Hernández, X. Han, M. Rico, L. Roso, C. Cascales, C. Zaldo, Opt. Express 23 (2015) 11135-11140.
25. J.M. Serres, P. Loiko, X. Mateos, K. Yumashev, N. Kuleshov, V. Petrov, U. Griebner, M. Aguiló, F. Díaz, Opt. Mater. Express 5 (2015) 661-667.
26. A. S. Yasyukevich, V. G. Shcherbitskii, V. E. Kisel, A. V. Mandrik, N. V. Kuleshov, J. Appl. Spectr. 71 (2004) 202–208.
27. T. T. Basiev, A. A. Sobol, P. G. Zverev, L. I. Ivleva, V. V. Osiko, R. C. Powell, Opt. Mater. 11 (1999) 307–314.
28. A.A. Kaminskii, K. Ueda, H. E. Eichler, J. Findeisen, S. N.Bagayev, F. A. Kuznetsov, A. A. Pavlyuk, G. Boulon, F. Bourgeois, Jpn. J. Appl. Phys. 37 (1998) L923-L926.
29. L. Macalik, J. Hanuza, A. A. Kaminskii, J. Mol. Struct. 555 (2000) 289–297.
30. K. van Dalfsen, S. Aravazhi, C. Grivas, S. M. García-Blanco, M. Pollnau, Opt. Lett. 39 (2014) 4380-4383.
31. P. Loiko, J. M. Serres, X. Mateos, H. Yu, H. Zhang, J. Liu, K. Yumashev, U. Griebner, V. Petrov, M. Aguiló, F. Díaz, IEEE Photonics J. 8 (2016) 1501312-1–12.
32. P.A. Loiko, X. Mateos, N.V. Kuleshov, A.A. Pavlyuk, K.V. Yumashev, V. Petrov, U. Griebner, M. Aguiló, F. Díaz, IEEE J. Quantum Electron. 50 (2014) 669-676.
33. M. Mączka, J. Sol. State Chem. 129 (1997) 287-297.
34. P. V. Klevtsov, R. F. Klevtsova, J. Struct. Chem. 18 (1977) 339–355.

Figure captions

Figure 1 (a,b) Photographs of the as-grown Yb,In:KLuW (a) and Yb,In:KYW (b) crystals; (c) their morphology; and (d) orientation of crystallographic (***a***, ***a****, ***b***, ***c***) and optical indicatrix (N_p, N_m, N_g) axes.

Figure 2 Absorption, σ_{abs}, stimulated-emission, σ_{SE}, (a,b) and gain, σ_g, (c,d) cross-sections of Yb,In:KLuW for light polarization $E \parallel N_m$ (a,c) and $E \parallel N_p$ (b,d), β: inversion ratio.

Figure 3 Absorption, σ_{abs}, stimulated-emission, σ_{SE}, (a,b) and gain, σ_g, (c,d) cross-sections of Yb,In:KYW for light polarization $E \parallel N_m$ (a,c) and $E \parallel N_p$ (b,d), β: inversion ratio.

Figure 4 Decay of the luminescence of Yb,In:KLuW (a) and Yb,In:KYW (b) crystals: The excitation is at 980 nm, the luminescence is at 1040 nm. The samples are 10 wt.% powder immersed in glycerin. *Symbols* – experimental data, *solid lines* – single-exponential fits.

Figure 5 Comparison of the emission spectra of Yb,In:KLuW and Yb:KLuW (a,b), and Yb,In:KYW and Yb:KYW (c,d) crystals for light polarizations $E \parallel N_m$ (a,c) and $E \parallel N_p$ (b,d). The excitation is at 940 nm (marked by an arrow).

Figure 6 Polarized Raman spectra of Yb,In:KLuW for *p*(*xx*)*p* (a), *m*(*xx*)*m* (b) and *g*(*xx*)*g* (c) geometries. The excitation wavelength is 632.8 nm.

Figure 7 Comparison of the Raman spectrum of Yb,In:KLuW with Yb,In:KYW (a) and Yb:KLuW (b). The excitation wavelength is 632.8 nm.

Figure 8 (a) Input-output dependences of the Yb,In:KLuW microchip laser: *Symbols*: experimental data, *lines*: fits for the calculated slope efficiency (η); (b) typical laser emission spectra for P_{abs} = 5 W.

Figure 9 Polarization-switching of the Yb,In:KLuW microchip laser: Output power (a) and laser emission spectra (b) for the $E \parallel N_m$ and $E \parallel N_p$ oscillation states, T_{OC} = 1%.

Figure 10 (a) Intensity profiles of the laser beam along the N_m and N_p-axes, *symbols* – experimental data, *curves* – Gaussian fits, R^2 – quality of the fit, *inset*: 2D spatial beam profile; (b) evaluation of the M^2 factors of the laser beam, T_{OC} = 5%, P_{abs} = 7 W.

Figure 1

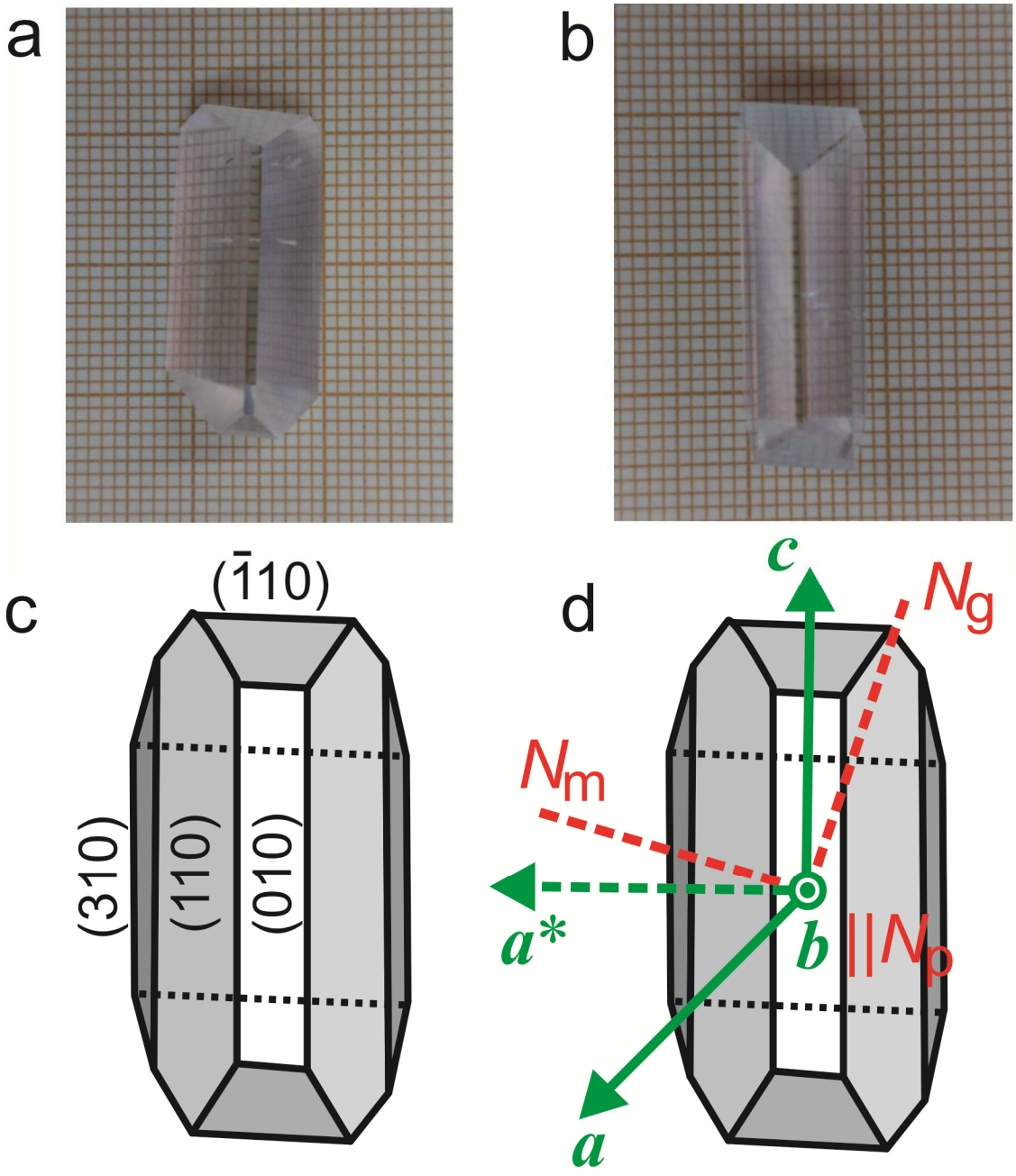

Figure 2

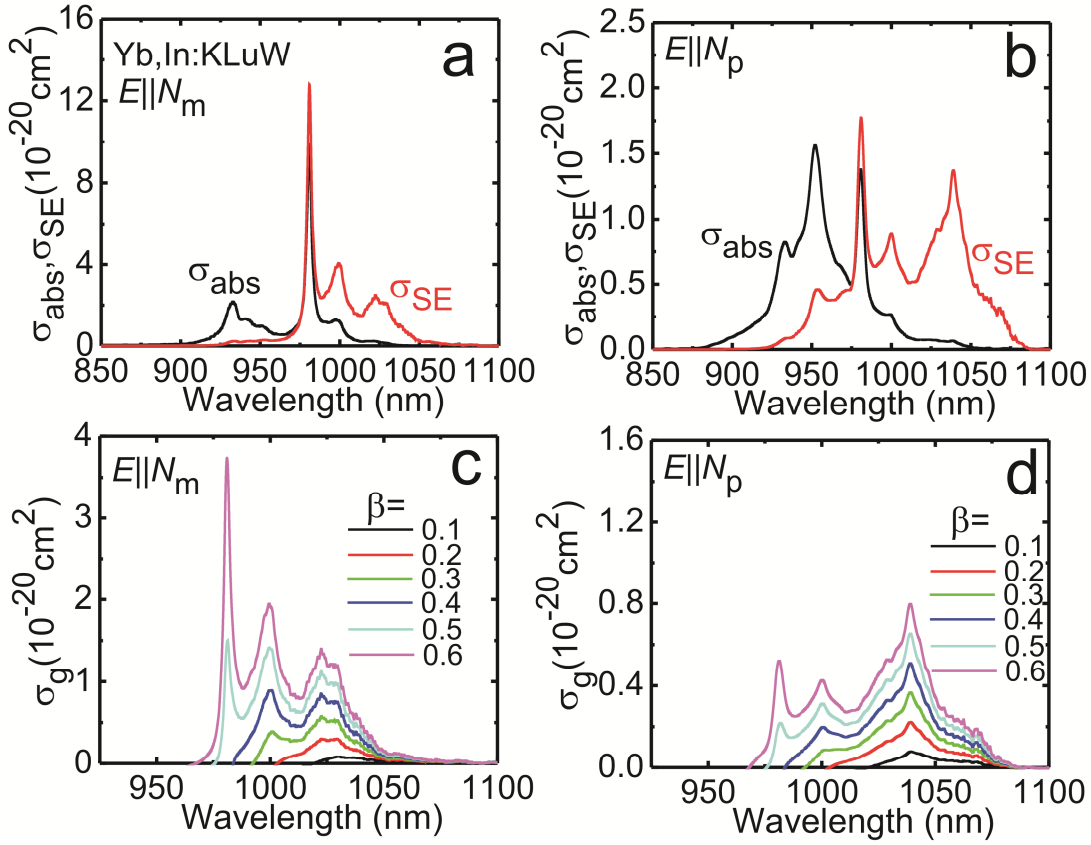
Yb,In:KLuW
E||Nm
a
σabs
σSE
σabs,σSE(10-20cm2)
Wavelength (nm)
E||Np
b
c
β=
0.1
0.2
0.3
0.4
0.5
0.6
σg(10-20cm2)
d

Figure 3

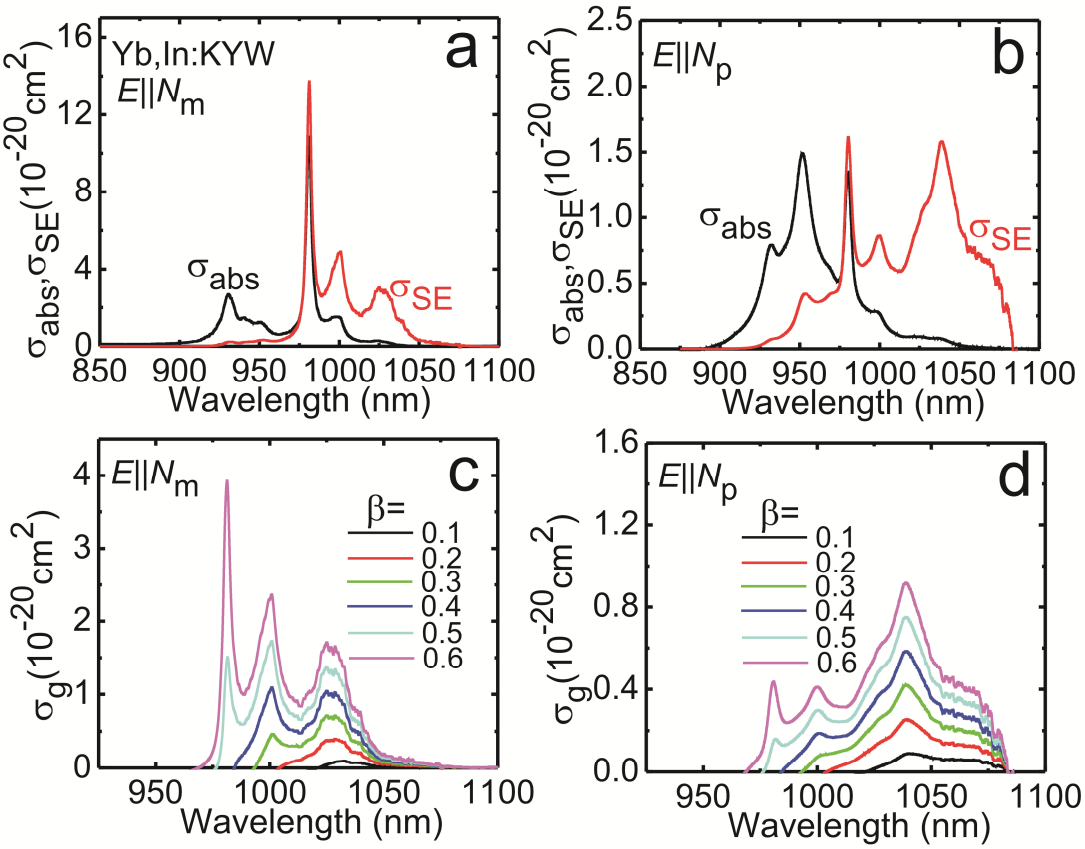

Figure 4

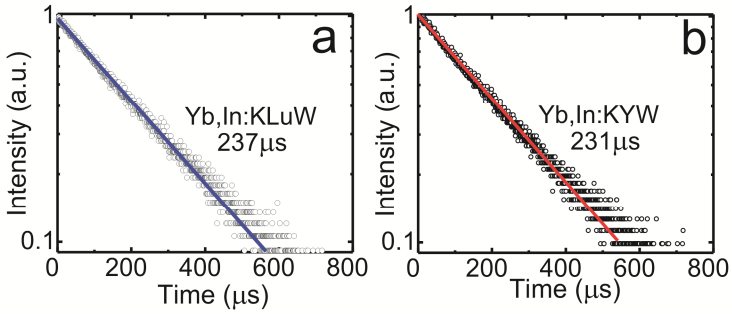

Figure 5

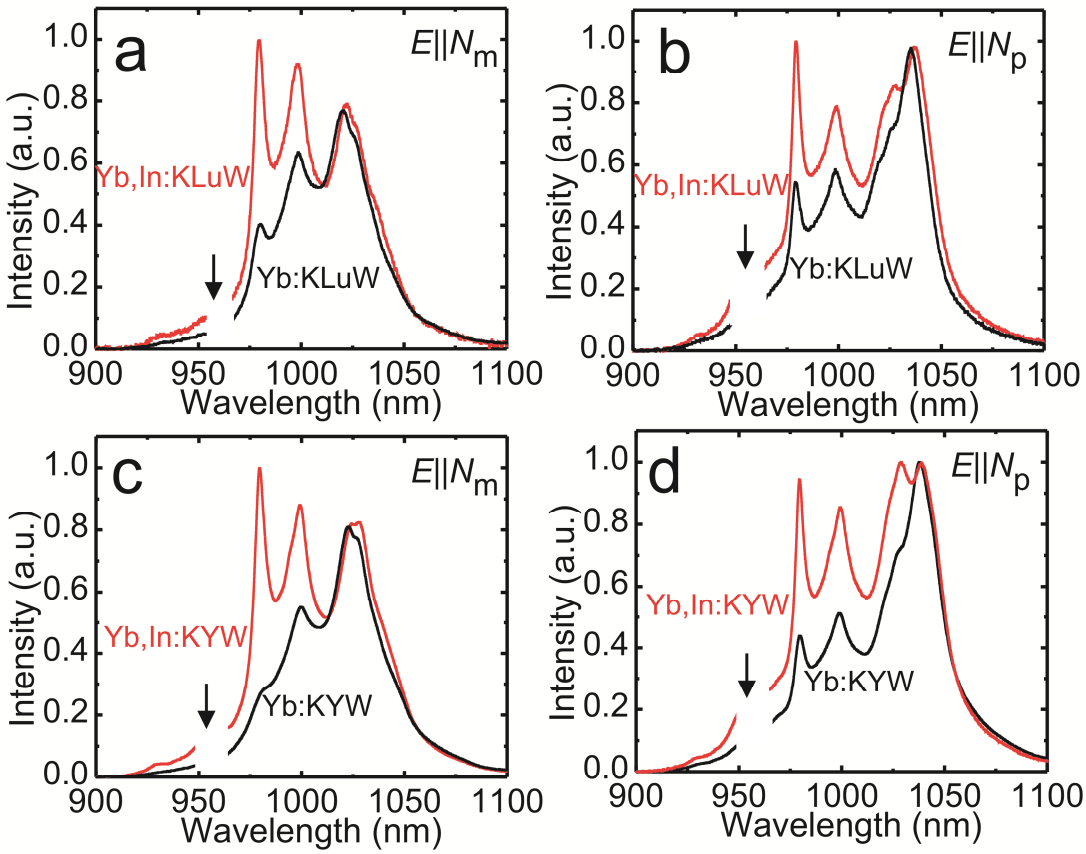
a
E||N_m
Yb,In:KLuW
Yb:KLuW
b
E||N_p
Yb,In:KLuW
Yb:KLuW
c
E||N_m
Yb,In:KYW
Yb:KYW
d
E||N_p
Yb,In:KYW
Yb:KYW
Intensity (a.u.)
Wavelength (nm)
0.0
0.2
0.4
0.6
0.8
1.0
900
950
1000
1050
1100

Figure 6

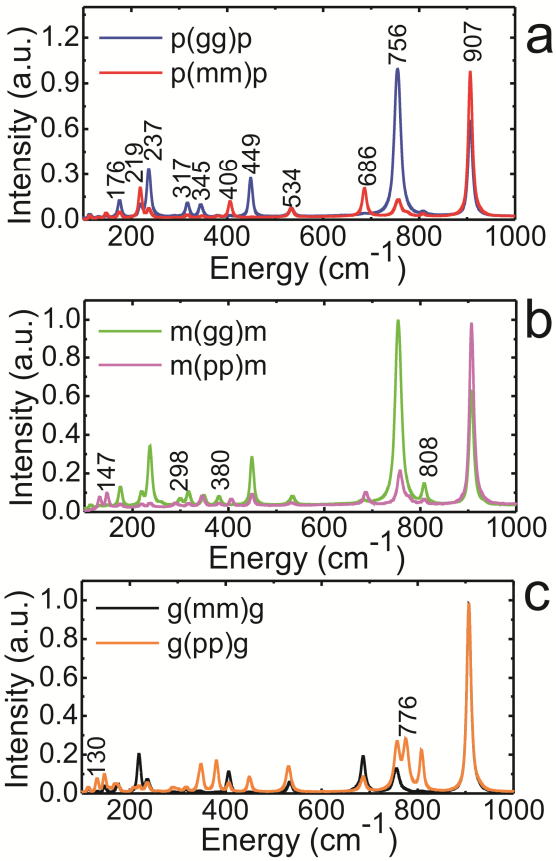

Figure 7

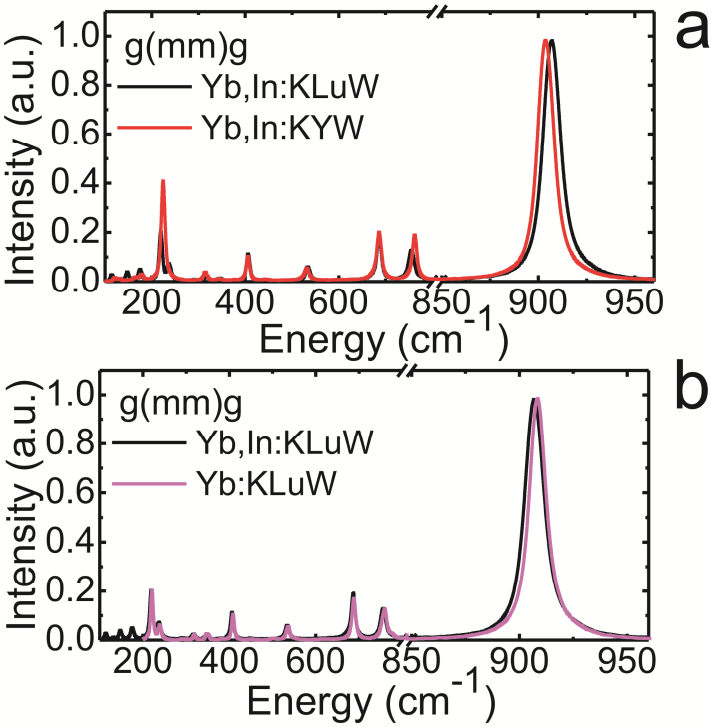

Figure 8

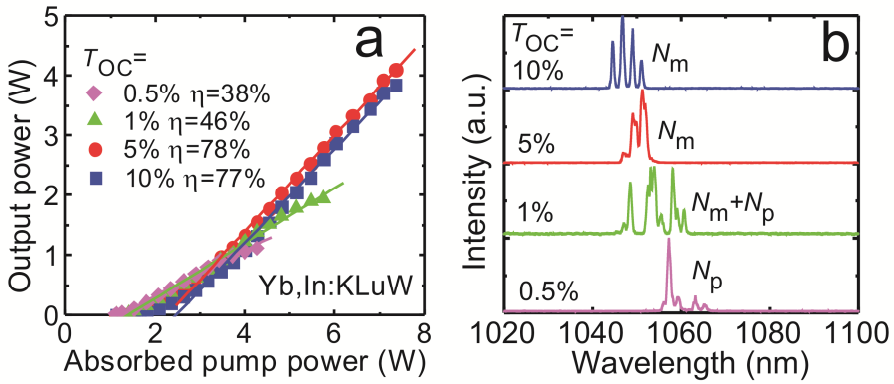

Figure 9

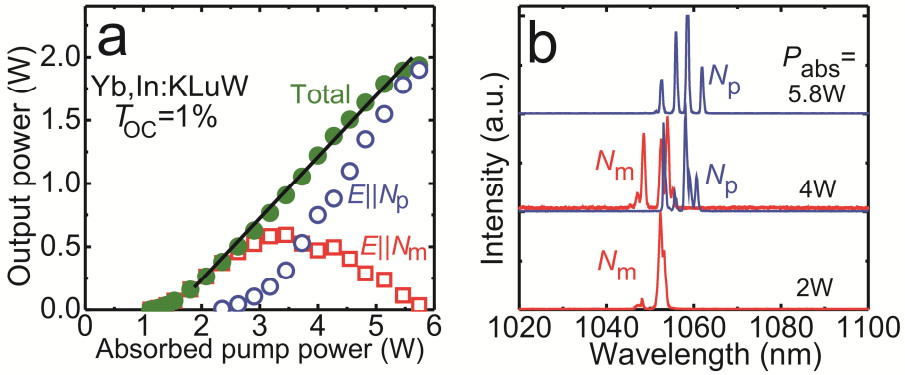

Figure 10